Phase advance and beta function measurements using Model-Independent Analysis

Chun-xi Wang,* Vadim Sajaev, and Chih-Yuan Yao
Argonne National Laboratory, 9700 South Cass Avenue, IL 60439
(Dated: December 20, 2002)

Phase advance and beta function are basic lattice functions characterizing the linear properties of an accelerator lattice. Accurate and efficient measurements of these quantities are important for commissioning and operating a machine. In this paper, we briefly review commonly used methods for measuring these lattice functions and develop a new method by extending the Model-Independent Analysis technique. The new method uses beam histories of excited betatron oscillations measured simultaneously at a large number of beam position monitors. It is fast, accurate, and robust. Measurements done at the storage ring of the Advanced Photon Source are reported. Comparisons among various methods are made.

I. INTRODUCTION

Beam orbits in an accelerator are usually dominated by the linear properties of its lattice. In most lattices, coupling between the two transverse degrees of freedom are kept at a minimum. Thus, to a good approximation, a transverse orbit can usually be described by

$$x(s) = x_0(s) + x_\beta(s) + D_x(s)\,\delta, \tag{1}$$

where x_0 is the 0-th order orbit around which occur small betatron oscillations x_β and oscillations coupled from the energy δ oscillation through the dispersion D_x. Here x represents either horizontal or vertical beam positions. In this paper we will ignore transverse coupling. The betatron oscillation can be described by the well-known expression

$$x_\beta(s) = \sqrt{2J\,\beta(s)}\cos[\phi + \psi(s)], \tag{2}$$

where $\{J, \phi\}$ are the action-angle variables specifying a specific orbit, $\beta(s)$ is the beta function, and $\psi(s)$ is the phase advance. The lattice functions β and ψ as well as D_x characterize the linear properties of a lattice. It is an important and routine task to measure these lattice functions. The transverse orbit information is primarily collected from a large number of beam position monitors (BPMs) along a machine. Various methods have been developed to derive the lattice functions from BPM measurements. Some depend on narrow-band BPMs that can measure only the closed orbits; others use broad-band BPMs capable of measuring beam histories on a turn-by-turn basis.

In recent years, Model-Independent Analysis (MIA) emerged as a new approach to study beam dynamics by analyzing simultaneously recorded beam histories at a large number of BPMs [1, 2]. A basic technique used in MIA is the spatial-temporal mode analysis via a singular value decomposition (SVD) of the data matrix containing beam histories. Similar to the Fourier analysis, SVD mode analysis decomposes the spatial-temporal variation of the beam centroid into superposition of various orthogonal modes by effectively accomplishing a major statistical data analysis, namely the Principal Component Analysis [3, 4]. Let b_p^m represents the measurement at the m-th monitor for the p-th pulse or turn. Then the singular value decomposition of the beam-history matrix $B_{P\times M} = \left(b_p^m\right)$ gives

$$B = USV^T = \sum_{\text{modes}} \sigma_i u_i v_i^T, \tag{3}$$

where $U_{P\times P} = [u_1, \cdots, u_P]$ and $V_{M\times M} = [v_1, \cdots, v_M]$ are orthonormal matrices comprising the temporal and spatial eigenvectors, and $S_{P\times M}$ is a rectangular matrix with nonnegative singular values σ_i along the upper diagonal. A pair of spatial and temporal vectors characterizes an eigenmode and the corresponding singular value specifies the overall amplitude of the eigenmode. In this paper, we will show that when beam motion is dominated by betatron oscillations, there are two orthogonal eigenmodes corresponding to the normalized coordinates that are normally used to describe the betatron motion. From these two betatron modes, the phase advance and beta function can be derived with good accuracy. The new method is applicable to both linacs and rings. However, our discussion here is focused on rings since our experiments were carried out at the storage ring of the Advanced Photon Source (APS).

This paper is organized as follows. First we briefly review commonly used methods for measuring beta function and phase advance. Then we show that the SVD eigenmodes yield the betatron modes, from which the lattice functions are derived. After discussion of the simple theory of our technique, we report experiments done at the APS storage ring. Based on our experience, we compare our technique with commonly used ones and argue certain advantages of our technique.

II. COMMON TECHNIQUES TO MEASURE LATTICE FUNCTIONS

In this section we briefly review common techniques used to measure beta functions and phase advances [2, 5,

*wangcx@aps.anl.gov

6]. Emphasis is on the basic concept of each technique for better appreciation of the technique developed in this paper.

A. Quadrupole scan and corrector scan

The most basic techniques to measure beta function are based on varying a quadrupole or a dipole corrector and deducing the beta function at the magnets. When the gradient of a quadrupole is perturbed by Δk_x, the tunes will be perturbed by $\Delta\mu$, and the beta function can be determined as

$$\beta_{x,y} \simeq \pm 4\pi \frac{\Delta\mu_{x,y}}{\Delta k_x}. \tag{4}$$

By measuring the tune change against quadrupole strength change, one can measure the beta function at the quadrupole. When a corrector generates an angular kick $\Delta\theta$, the closed orbit will be perturbed by $\Delta x_{c.o.}(s)$. By measuring this deviation at a nearby (negligible phase advance in between) BPM, the beta function at the corrector or BPM can be determined as

$$\beta_x \simeq 2\tan\pi\mu \, \frac{\Delta x_{c.o.}}{\Delta\theta}. \tag{5}$$

For better measurement, the magnets are scanned and the beta function is measured by fitting the slope of tune or orbit deviation. Both methods are quite simple but slow (especially when a large number of magnets are used) and require independently powered magnets with reliable calibration.

B. Harmonic analysis of orbit oscillation

The above methods are based on closed orbits measured with narrow-band BPMs. A faster technique based on orbit oscillations measured with broadband BPMs was developed and successfully used to measure the phase advances and beta function in LEP (Large Electron Position Collider at CERN) [7, 8]. A similar technique was implemented in CESR (the Cornell Electron/Position Storage Ring), where a signal analyzer effectively accomplished the harmonic analysis [9]. Our discussion here is based on the LEP approach. At a given BPM, an ideal betatron oscillation recorded at the n-th turn can be written as

$$x_n = A\cos(2\pi n\mu_x + \psi), \tag{6}$$

where A is the oscillation amplitude, μ_x is the tune, and ψ is the phase. It is easy to see that

$$s = \sum_{n=1}^{N} x_n \sin(2\pi n\mu_x) \xrightarrow{\text{large } N} -\frac{AN}{2}\sin\psi, \tag{7}$$

$$c = \sum_{n=1}^{N} x_n \cos(2\pi n\mu_x) \xrightarrow{\text{large } N} \frac{AN}{2}\cos\psi. \tag{8}$$

Therefore the phase at the given BPM can be determined by

$$\psi \simeq -\tan^{-1}\left(\frac{s}{c}\right). \tag{9}$$

To determine the phase via Eqs. (7) and (8), a very accurate tune measurement is required (10^{-5} quoted at LEP) [8]. To determine the phase advances between BPMs, the BPMs must be synchronized so that all the phases reference to the same point.

From the phase advances and the transfer matrix between BPMs, beta function can be determined independent of BPM gain calibration. For any given three BPMs, the beta function at the first BPM can be written as [8]

$$\beta_1 = \frac{\cot\psi_{12} - \cot\psi_{13}}{(m_{11}/m_{12}) - (n_{11}/n_{12})}, \tag{10}$$

where m_{11} and m_{12} are the elements of the first row of the transfer matrix from the 1st to the 2nd BPMs; similarly, n_{11} and n_{12} are those from the 1st to the 3rd BPMs. Although Eq. (10) does not rely on BPM calibrations, it does rely on the correctness of the transfer matrices and thus becomes unreliable in regions with focusing errors. More sophisticated analysis of phase advance and beta function have been used at CESR [10].

C. Model calibration via the response matrix method

The above methods measure the phase advance and beta function directly. There are methods that build a machine model based on measurements, and the phase advance and beta function are byproducts of the model. The response-matrix method is a systematic method to calibrate accelerator models and has been successfully used on many machines [11–15]. The basic idea is to minimize the difference between measured and calculated (from a model) BPM responses to changes in steering magnet strengths by adjusting various model parameters such as corrector strengths, quadrupole gradients, and BPM gains. This idea can be formulated as follows. For any given magnetic steering θ_x and θ_y, responses at BPMs can be measured as well as calculated according to one's model to generate the response matrices R^{meas} and R^{mod} so that

$$\begin{pmatrix} x \\ y \end{pmatrix} = R^{\text{meas or mod}} \begin{pmatrix} \theta_x \\ \theta_y \end{pmatrix}, \tag{11}$$

where x and y are the beam orbit response. Such a response matrix can be extended to cover all M BPMs and N steering magnets, so that there are $M \times N$ elements. The figure to be minimized can be specified by

$$\chi^2 = \sum_{i,j} \frac{\left(R_{ij}^{\text{meas}} - R_{ij}^{\text{mod}}(\xi_1, \xi_2, \cdots)\right)^2}{\sigma_i^2}, \tag{12}$$

where i goes through all BPMs of resolution σ_i, and j goes through all steering magnets. The ξ's are model parameters to be adjusted for the minimization.

In addition, BPM gains and corrector scaling factors can be introduced to correct the measured response matrix, i.e., use $BR^{\rm meas}C$ to replace the $R^{\rm meas}$ in the above expression, where the diagonal matrix B contains BPM gains and C contains corrector scaling factors. Further correction factors can be added when necessary. For example, the following BPM correction scheme is used in LOCO [13] for each BPM:

$$\begin{pmatrix} \bar{x} \\ \bar{y} \end{pmatrix} = \frac{1}{\sqrt{1-c^2}} \begin{pmatrix} \cos\theta & \sin\theta \\ -\sin\theta & \cos\theta \end{pmatrix} \begin{pmatrix} 1 & c \\ c & 1 \end{pmatrix} \begin{pmatrix} g_x x \\ g_y y \end{pmatrix}, \quad (13)$$

where g is the gain, θ is the roll angle, and c is a factor due to BPM pick-up electrodes layout. All such factors can be varied for the minimization.

The implementation details of the response-matrix method could be quite different depending on how sophisticated one's model is. Typically there are thousands of response-matrix elements and hundreds of model parameters used for the optimization. In general, the beam responses could be nonlinear, thus minimization over such a large parameter space could become difficult, if not senseless, and time consuming. One way to solve the minimization problem is to linearize the response as

$$R_{ij}^{\rm mod} = R_{ij}^0 + \sum_{\{\xi\}} \frac{\partial R_{ij}}{\partial \xi}\, \delta\xi \quad (14)$$

and obtain the solution using the least-squares fitting

$$\delta\vec{\xi} = (A^T A)^{-1} A^T \left[R_{ij}^{\rm meas} - R_{ij}^0\right]_{M\times N,1}, \quad (15)$$

where matrix $A = \left[\frac{\partial R_{ij}}{\partial \xi}\right]$ consists of the $M \times N$ derivatives over each parameter in a column, and the number of columns depends on the number of parameters in use. Usually A is quite a large matrix. Often such procedures need to be iterated due to the presence of nonlinear responses. The response-matrix method has proven successful in calibrating the linear models of many light source storage rings.

Note that the design matrix A is generated from one's model; therefore, a good model is crucial. If there is a sufficient number of BPMs and a good model is available, the response-matrix method provides a systematic and powerful tool to calibrate model parameters. However, the response-matrix method may not work well in cases where unanticipated physics affect the beam response and are not included in the model.

D. Model calibration using beam histories

A still-evolving model calibration method is being developed for PEP-II at SLAC [16, 17]. Unlike the response-matrix method where a large number of measured closed-orbit distortions are used to fit with a model, only four high-quality linearly independent betatron orbits are extracted from simultaneously acquired beam histories at all BPMs. In principle, these four orbits contain all linear lattice information obtainable from BPMs because any other linear orbit in the four-dimensional transverse phase space is a linear superposition of those four orbits. For any pair of these four orbits there is a Lagrange invariant [18]

$$\mathcal{L}_{ij} = (x_i x_j' - x_j x_i') + (y_i y_j' - y_j y_i'), \quad 1 \le i, j \le 4, \quad (16)$$

where the prime means derivative (here we view x' and y' as canonical momentum). Due to the antisymmetric construct, only six independent invariants exist. In one degree of freedom, it is the same as the Wronskian. From the four betatron orbits and the Lagrange invariants, the linear Green's function elements R_{12}, R_{14}, R_{32}, and R_{34} of the transfer matrix R^{ba} from location a to b can be computed as

$$\begin{pmatrix} R_{12}^{ba} & R_{14}^{ba} \\ R_{32}^{ba} & R_{34}^{ba} \end{pmatrix} = Z^b L^{-1} Z^{aT}, \quad (17)$$

where $Z = \begin{pmatrix} x_1 & x_2 & x_3 & x_4 \\ y_1 & y_2 & y_3 & y_4 \end{pmatrix}$ containing beam positions of all four orbits, and $L = (\mathcal{L}_{ij})$ containing all Lagrange invariants. See Ref. [16] or Appendix A for proof of Eq. (17). Note that R_{12}^{ba} involves only x^b and x^a, R_{14}^{ba} involves only x^b and y^a, and so on. The measurements at locations a and b determine which R-matrix element can be measured. The Lagrange invariants depend on the lattice as well as beam excitations. If the first (last) two orbits come from horizontal (vertical) machine eigenmodes, only $\mathcal{L}_{12}$ and $\mathcal{L}_{34}$ are nonzero. Thus the right-hand side of Eq. (17) can be significantly simplified.

The measured Green's function elements can be fitted with a model that incorporates magnet errors as well as gains and rolls of BPMs. An obvious advantage of using beam histories is that it takes a much shorter time to acquire the data. Furthermore, since the measured R-matrix elements are localized, fitting with model can be localized as well, thus eliminating the need to deal with a huge response matrix. Like the response-matrix method, successful model calibration requires a good machine model and a sufficient number of BPMs.

III. MIA TECHNIQUE TO MEASURE LATTICE FUNCTIONS

A. Betatron modes and SVD eigenmodes

As mentioned in the introduction, SVD analysis of the beam-history matrix decomposes the spatial-temporal variation of beam betatron orbits into orthogonal eigenmodes. Two of them are betatron modes that characterize the betatron motion. In this section we prove

this statement by analytically computing the SVD eigenmodes of a linear system given by Eq. (2). For simplicity, BPM noise is ignored here. In such a system, the m-th BPM reading for the p-th pulse can be expressed in action-angle variables $\{J_p, \phi_p\}$ as

$$b_p^m = \sqrt{2J_p\beta_m}\cos(\phi_p + \psi_m), \tag{18}$$

where β_m is the beta function at the m-th BPM, and ψ_m is the phase advance from a starting point to the m-th BPM. Note that a subscript p is given to the action and angle variables. In a linac, this accounts for the different initial conditions of each pulse. In a ring, it accommodates action and angle variations from turn to turn. For an ideal linear system, the action is conserved and the angle simply advances by the tune each turn. However, nonlinear effects and damping of the beam centroid can lead to much more complicated action-angle variation although they do not deviate much within each turn.

Now let us compute the eigenmodes analytically. For convenience, we use $B = (b_p^m)/\sqrt{P}$ so that the variance-covariance matrix is simply given by $C_B = B^T B$. From the BPM data given by Eq. (18), the elements of C_B read

$$\begin{aligned}(C_B)_{mn} &= \frac{1}{P}\sum_{p=1}^{P} b_p^m b_p^n \\ &= \sum_{p=1}^{P}\frac{J_p}{P}\sqrt{\beta_m\beta_n}\left[\cos(\psi_m-\psi_n)+\cos(2\phi_p+\psi_m+\psi_n)\right] \\ &= \langle J\rangle_p\sqrt{\beta_m\beta_n}\,\cos(\psi_m-\psi_n),\end{aligned} \tag{19}$$

where $\langle J\rangle_p$ is the ensemble average of the action. The subscript p is dropped hereafter. The last term involving ϕ_p averages to zero for sufficiently large P. From Eq. (3),

$$C_B V = \left(USV^T\right)^T\left(USV^T\right)V = VS^2, \tag{20}$$

thus, the spatial vectors of B are the eigenvectors of C_B and the singular values are the square roots of the eigenvalues of C_B, i.e., $\sigma = \sqrt{\lambda}$.

To find eigenvalues and eigenvectors of C_B, we need to solve for ϕ_0 such that the corresponding orbit $v = \{\sqrt{2J\beta_m}\cos(\phi_0+\psi_m), m = 1,\cdots,M\}$ satisfies the secular equation

$$C_B\, v = \lambda\, v\,. \tag{21}$$

From the m-th component of the secular equation,

$$\begin{aligned}&\lambda\cos(\phi_0+\psi_m) \\ =\;& \langle J\rangle\sum_{n=1}^{M}\beta_n\cos(\psi_m-\psi_n)\cos(\phi_0+\psi_n) \\ =\;& \langle J\rangle\left[\cos(\phi_0+\psi_m)\sum_{n=1}^{M}\beta_n\cos^2(\phi_0+\psi_n)\right. \\ &\left.+\frac{1}{2}\sin(\phi_0+\psi_m)\sum_{n=1}^{M}\beta_n\sin 2(\phi_0+\psi_n)\right].\end{aligned} \tag{22}$$

Therefore, we have the condition

$$\sum_{n=1}^{M}\beta_n\sin 2(\phi_0+\psi_n) = 0. \tag{23}$$

There are two solutions,

$$\phi_0 = -\frac{1}{2}\arctan\left(\frac{\sum_n\beta_n\sin 2\psi_n}{\sum_n\beta_n\cos 2\psi_n}\right) \tag{24}$$

and $\phi_0 + \frac{\pi}{2}$, that lead to two different eigenvectors. The two eigenvalues are

$$\lambda_\pm = \frac{1}{2}\langle J\rangle\left[\sum_{n=1}^{M}\beta_n + \sum_{n=1}^{M}\beta_n\cos 2(\phi_0+\psi_n)\right] = \frac{1}{2}\langle J\rangle\left[\sum_{n=1}^{M}\beta_n \pm \sqrt{\left(\sum_n\beta_n\cos 2\psi_n\right)^2+\left(\sum_n\beta_n\sin 2\psi_n\right)^2}\right] \tag{25}$$

Note that the leading term is proportional to $M\langle J\rangle_p\langle\beta\rangle_m$ that grows with the number of BPMs used. Thus it is often convenient to remove such dependence when using singular values. The normalized eigenvectors are

$$\begin{cases} v_+ = \frac{1}{\sqrt{\lambda_+}}\left\{\sqrt{\langle J\rangle\beta_m}\cos(\phi_0+\psi_m),\ m=1,\cdots,M\right\} \\ v_- = \frac{1}{\sqrt{\lambda_-}}\left\{\sqrt{\langle J\rangle\beta_m}\sin(\phi_0+\psi_m),\ m=1,\cdots,M\right\}. \end{cases} \tag{26}$$

These two vectors are obviously orthogonal according to Eq. (23). The normalized temporal vectors that are consistent with the spatial vectors are

$$\begin{cases} u_+ = \left\{\ \sqrt{\frac{2J_p}{P\langle J\rangle}}\cos(\phi_p-\phi_0)\ ,\ p=1,\cdots,P\right\} \\ u_- = \left\{-\sqrt{\frac{2J_p}{P\langle J\rangle}}\sin(\phi_p-\phi_0)\ ,\ p=1,\cdots,P\right\}, \end{cases} \tag{27}$$

which clearly relate to the commonly used normalized coordinates! Note that the orthogonality of these two vectors holds for $P\to\infty$. In other words, for finite P, these expressions are only approximate. So is Eq. (19).

In summary, the SVD of the beam-history matrix of the betatron oscillation is given by

$$B \equiv \frac{1}{\sqrt{P}} \left(b_p^m\right) = \sigma_+ u_+ v_+^T + \sigma_- u_- v_-^T \,, \qquad (28)$$

where the singular values $\sigma_\pm = \sqrt{\lambda_\pm}$, and the spatial and temporal singular vectors are the column vectors given by Eqs. (26) and (27). Remarkably, the SVD yields the well-known normalized coordinates for this 1-D dynamical system. Note that there is a sign ambiguity in the singular vectors. By definition the singular values are non-negative and singular vectors are normalized to one. But for a pair of singular vectors u and v, their negatives, $-u$ and $-v$, can also be chosen as the singular vectors.

In practice the measured beam histories contain not only the dominating betatron oscillation but also BPM noises as well as motions due to other small perturbations. It is difficult to analytically study the eigenmodes for more complicated systems. Nonetheless, there is a matrix theorem that states that $O(\epsilon)$ changes in B can alter a singular subspace by an amount ϵ/Δ, where Δ measures the separation of the relevant singular values [19]. Thus, as long as the the singular values of the betatron modes are far from the rest, Eq. (28) should be a good representation of the measured betatron modes.

B. Determination of phase advance and beta function

From the betatron vectors, Eq. (26), the phase advances can be determined as

$$\psi = \tan^{-1}\left(\frac{\sigma_- v_-}{\sigma_+ v_+}\right), \qquad (29)$$

where the phase ϕ_0 is absorbed by shifting the reference point of the phase. Since we are interested in only the phase advance between BPMs, the reference point does not matter. The beta function can be written as

$$\beta = \langle J \rangle^{-1} \left(\lambda_+ v_+^2 + \lambda_- v_-^2\right). \qquad (30)$$

Note that, except for an overall scaling factor $\langle J \rangle$ in β, the phase advance and beta function can be computed from the betatron vectors obtained by an SVD analysis of the beam-history matrix.

One complication in determining phase advances with Eq. (29) is the uncertainty due to the inversion of the triangular function and the sign ambiguity of the betatron vectors. Fortunately, the local phase-advance deviations from a machine model are generally much less than π, therefore, with estimated phase advances from even a crude machine model, the phase uncertainty can be resolved. Furthermore, it is not difficult to see that errors in BPM gains have no effect on the phase advance measurement since they will be cancelled in Eq. (29). In short, from the betatron vectors, the phase advances between BPMs can be uniquely determined, and the technique is model-independent and robust against BPM calibration errors.

It is difficult to obtain accurate error bounds for the measurements. However, the absolute errors in phase (in unit radian) and relative errors in beta function can be estimated by (see Appendix B)

$$\sigma_\psi \simeq \frac{1}{\sqrt{P}} \frac{\sigma_r}{\sigma_s} \quad \text{and} \quad \sigma_{\Delta\beta/\beta} \simeq 2\sigma_\psi, \qquad (31)$$

where σ_s is the rms strength of the betatron signal as measured by the singular values, and σ_r is the residual signal and noise that can be estimated by the quadratic sum of the singular values of non-betatron signals and random noise. For pure harmonic oscillations with random BPM noise, σ_r is BPM resolution and $\sigma_s = A/\sqrt{2}$, where A is the oscillation amplitude; then Eq. (31) is the same as errors quoted for the harmonic analysis [8]. The apparent P dependence loses its power quickly for a pulse signal, whose singular value decreases with $\sqrt{P}$ for large P. For sufficiently large P, the random noise becomes a secondary contribution to the error, and the $\sqrt{P}$ dependence will not hold any more. σ_r is difficult to estimate. Often the third largest singular value gives a rough estimate.

It is instructive to see the connection between the method developed here and the method based on harmonic analysis of orbit oscillations. For a perfect linear system without noise, the temporal vectors are pure harmonics and the spatial vectors are simply the coefficients of these harmonics. Thus, the two methods for phase-advance measurement are basically the same, although one uses harmonic analysis to extract the sine and cosine coefficients of the betatron oscillation in Eqs. (7, 8), and the other uses SVD to obtain the sine and cosine betatron orbits in Eq. (26). The apparent sign difference in Eqs. (9, 29) can be attributed to the sign ambiguity of the betatron vectors. However, the new method has the advantage that it requires neither a pure harmonic oscillation nor a very accurate tune measurement as input, since amplitude and phase variations can be tolerated in Eqs. (18, 27). Therefore, the method developed here is more robust and has wider applicability.

Computing beta function with Eq. (30), rather than simply using amplitude of individual BPMs, has the advantage that the extracted betatron modes are cleaner since non-betatron motion and noise have been excluded via mode analysis. However, one obvious limitation is that it depends on BPM gain calibration. Unfortunately, there is no simple way around this except fitting with machine models as described above.

IV. MEASUREMENTS DONE AT THE APS

To test the new method, experiments have been done at the APS storage ring using beam history measurements at 360 broadband BPMs with various kinds of beam excitations. Comparisons with the response-matrix

and harmonic-analysis methods have been made. Good agreements were reached.

A. Obtaining the betatron modes

With reliable measurements of beam histories, it is straightforward to extract the betatron modes as in Eq. (28) via SVD mode analysis. Unfortunately, the beam history modules of the current BPM system at the APS have various problems [20]. We will not discuss the details of confronting these problems with MIA. After identifying and removing the malfunctioning and noisy BPMs, about 3/4 of the 360 BPMs were used for the phase advance and beta function measurements. Another major obstacle is that these beam histories are not synchronized to the same turn. There is uncertainty about a couple of turns. It turns out that phase advance measurement is an effective technique to detect the synchronization problem. For each turn offset at a BPM, the phase advance is changed according to the tune. In order to avoid integer and half-integer resonances, the tune is usually much larger than the phase errors of the optics. Thus, by comparing the measured and designed phase advances, we are able to detect the out-of-sync beam histories and synchronize them by simply shifting the histories relative to each other (works for turn-by-turn but not for every-other-turn histories). The measured beam histories are further corrected with BPM gains obtained with the response-matrix method [15], which is necessary for beta function measurement. After the beam histories are cleaned, gain-corrected, and synchronized, a final SVD mode analysis is performed to extract the betatron modes–the first two eigenmodes that dominate the beam motion. Fourier analysis of the temporal patterns of the betatron modes are performed to confirm that the betatron modes are well separated from other modes due to synchrotron oscillation, transverse coupling, nonlinear effects in optics and BPMs, and so on. Here we will not report the details of all the modes we observed, although they are very informative.

B. Horizontal measurements with kick excitation

For the horizontal plane, an injection kicker is used to kick a stored bunch to a desired amplitude, and the resulting betatron oscillation is recorded. Mode analysis yields about ten modes above the noise floor: the two largest modes are the betatron modes, the third one is the synchrotron mode due to residual energy oscillation in the ring, and so on. As examples, the first and the third modes are shown in Figs. 1 and 2. The second betatron mode is similar to the first one. In Fig. 1, the spatial vector of the betatron mode is a betatron orbit. Due to the unusable BPMs (shown as red dots), the orbit is broken into pieces and looks irregular. The temporal vector clearly shows a beam that is kicked at about the

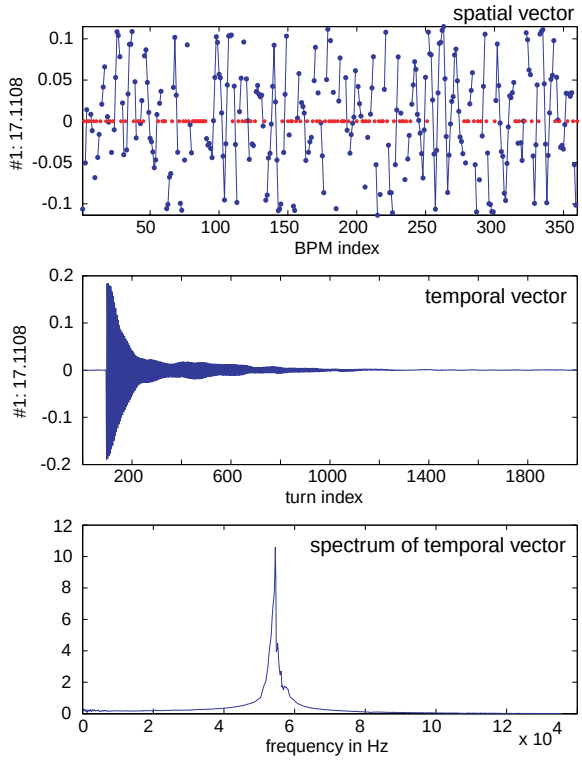

FIG. 1: The first horizontal mode with kick excitation. Measured values are plotted as solid dots and joined by lines for consecutive BPMs. Bad BPMs are indicated by dots at zero. The temporal vector shows time evolution of the beam.

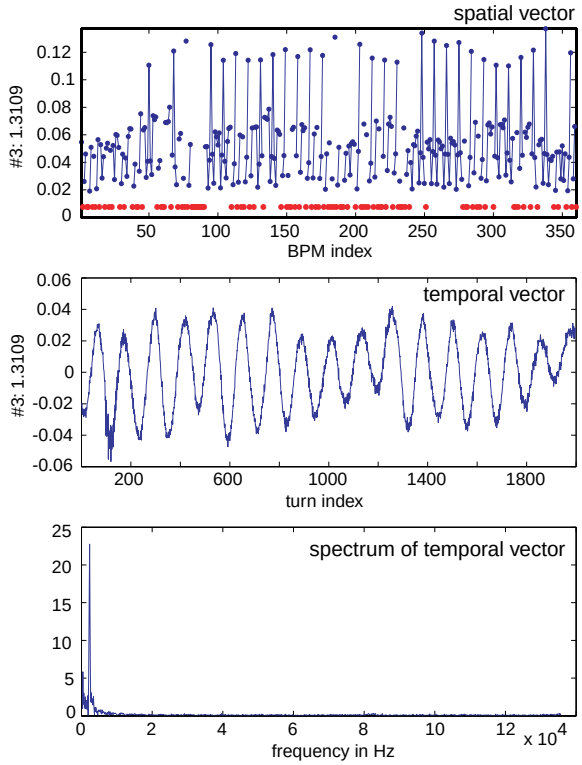

FIG. 2: The third horizontal mode: a synchrotron mode. See caption of Fig. 1 for more description.

100th turn then decohered and damped. By construct, both spatial and temporal vectors are normalized to one. The mode number and its singular value are shown on the left-hand-side label. The Fourier spectrum of the temporal vector shows the betatron frequency with a broadened peak due to decoherence. Note that the synchrotron and vertical tunes as well as other nonlinear resonance frequencies are invisible, even though they do exist and show up in other modes. This confirms the quality of the betatron modes. In Fig. 2, the spatial vector of the synchrotron mode (the third largest mode) corresponds to the dispersion. Again, the unusable BPMs broke the regular pattern. The temporal vector yields the residual energy oscillation in the ring, which is barely perturbed by the kick. The corresponding spectrum contains a clear synchrotron tune and various harmonics of the power line frequency.

The synchrotron mode and the noise floor are determined by the machine condition and BPM system, but independent of the kick strength. Increasing the kick strength improves the signal-to-noise ratio. However, due to decoherence, the oscillation is significantly damped in tens of turns, and the larger the kick amplitude the quicker it damps; thus the overall signal strength is limited.

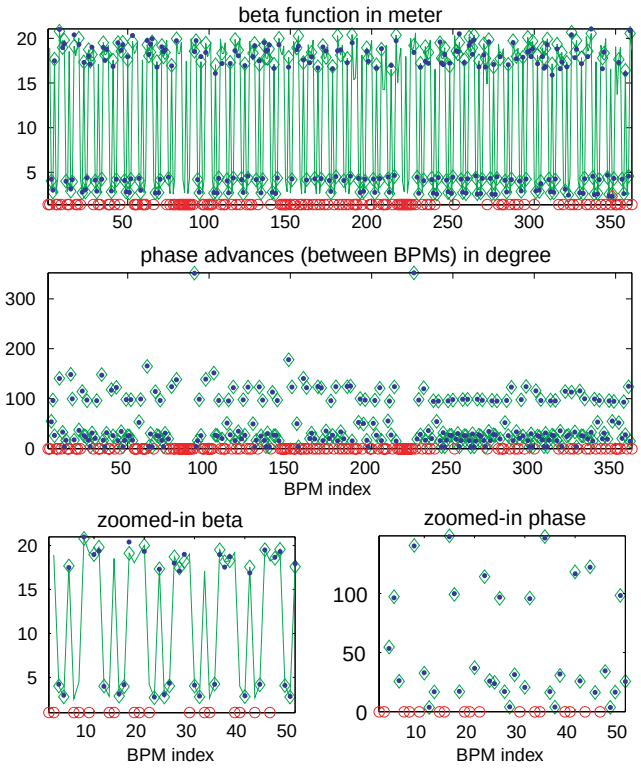

FIG. 3: Horizontal beta function and phase advance. The solid dots are MIA measurements. The solid lines are calibrated machine model. Diamonds are model values at used BPMs. Circles are malfunctioning BPMs. Figures in the third row are blowups of the above figures for the first 50 BPMs.

Using the spatial vectors of the two betatron modes and the procedure described in the last section, we obtained the phase advances and beta function for the horizontal plane as shown in Fig. 3. MIA measurement results are shown as solid dots. For comparison, corresponding model values are shown as diamonds. Instead of using a designed model, a fitted model with measured response matrix is used here. The standard deviations between these two are less than 4% for the beta function and 0.6° for the phase advances. These standard deviations contain measurement errors as well as actual differences in machine conditions for the measurements. Repeated MIA measurements yield repeatability about 0.7% for beta function and 0.33° for phase advances, which reflect the random errors of MIA measurements. In addition to the phase advances between BPMs, the cumulative phase is also examined for phase variation along the ring. The repeatability for cumulative phase is 0.24°. The phase advance between two BPMs is the difference of two cumulative phases, thus its error is $\sqrt{2}$ larger. These errors depend on excitation amplitudes and are limited by the maximum signal achievable in the presence of strong decoherence. Furthermore, at this level, the measurements become sensitive to slight changes in machine conditions from one measurement to another. For example, the machine tunes are only stable to the level of 10^{-3}, which is 0.36° in phase.

C. Vertical measurements with resonant excitation

For the vertical plane, we use a pinger to excite betatron oscillation. The pinger can be operated with either a high-voltage pulse drive or a low-voltage CW drive. Thus we can either kick the beam or resonantly excite the beam. With kick excitation, it is similar to the horizontal plane. Due to decoherence, it turns out that resonant excitation offers a stronger signal. Figure 4 shows the first betatron mode of a resonantly excited beam. As in Fig. 1, the spatial vector gives a vertical betatron orbit. The temporal vector shows a continuously excited beam, and its Fourier spectrum shows a much narrower peak at the betatron frequency. For various reasons, it is not easy to excite a pure harmonic oscillation in the APS ring when the data were taken. Thus the oscillation amplitude has significant variation, and the spectrum shows noticeable noise around the peak. A major difference between the horizontal and vertical planes is that there is no synchrotron mode in the vertical plane due to minute vertical dispersion.

The results for vertical beta function and phase advance are shown in Fig. 5. See the description of Fig. 3 for an explanation of the figure. In this vertical case, the standard deviations between model and measurements are less than 3% for the beta function and 0.5° for the phase advances. Repeatability is better than 0.6% for beta function, 0.21° for phase advances between BPMs, and 0.15° for cumulative phase (0.08° have been reached

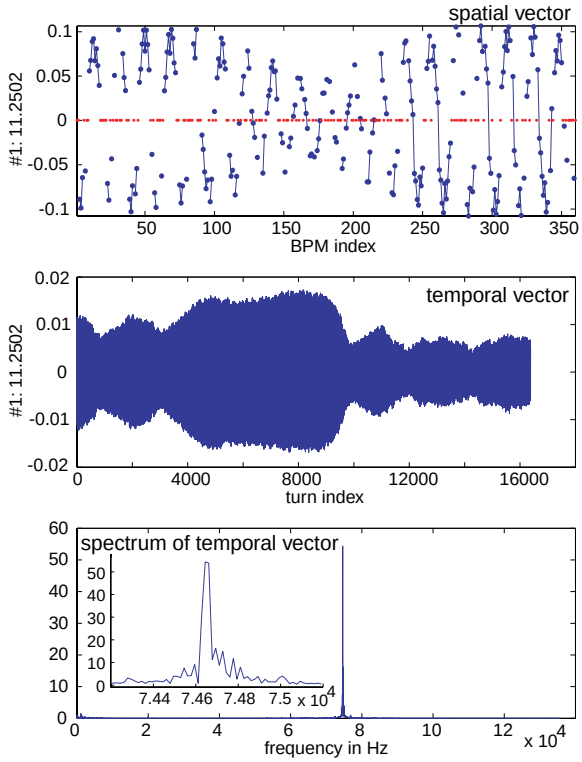

FIG. 4: The first vertical mode with resonant excitation. See caption of Fig. 1 for more description. Insert is a blowup.

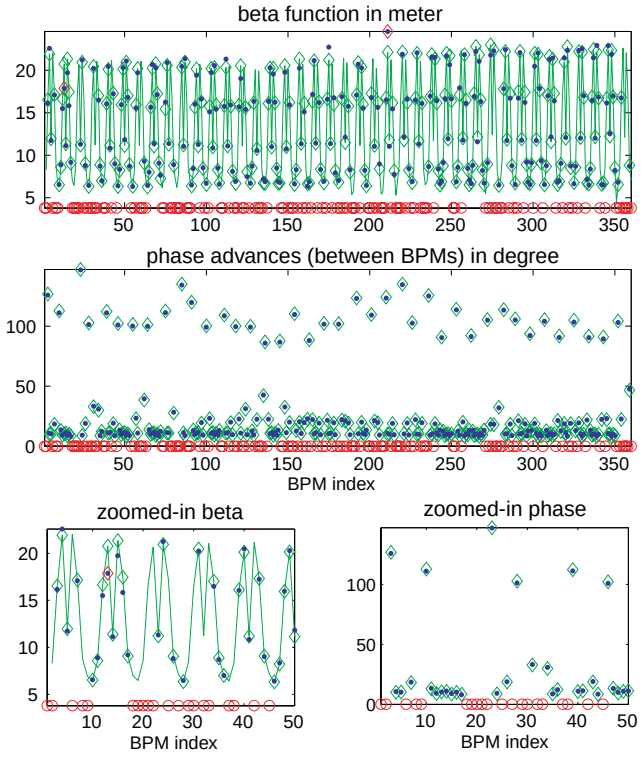

FIG. 5: Vertical phase advance and beta function. See caption of Fig. 3 for more description. The red diamond indicates those with deviations larger than 3σ.

with more coherent oscillation). Occasionally, there are significant difference at a few BPMs such as those marked in the figure. BPM gains are suspected, but we have not tracked down the exact cause. Since the response matrix measurement and the MIA measurement are carried out on different days, unexpected optics changes might also cause the differences.

For resonantly excited coherent oscillations, the harmonic analysis method can be used to determine the phase advances. For comparison, we did such an exercise and found that the standard deviation in phase advances between the harmonic analysis and MIA methods is less than 0.2°. The repeatability of harmonic analysis with carefully determined tune is about 0.2° for cumulative phase, slightly worse than the MIA method. Thus, the MIA method rivals the harmonic analysis method in accuracy and does not demand a predetermined accurate tune.

D. Measurement with excitation from instability

We showed measurements done with commonly used kick excitation and resonant excitation. In the APS storage ring, a single-bunch beam instability leads to a well-behaved bursting mode that has large periodic centroid oscillation [21]. Such a self-excited horizontal oscillation is also tested for measuring lattice functions. The first eigenmode is shown in Fig. 6. The temporal vector shows

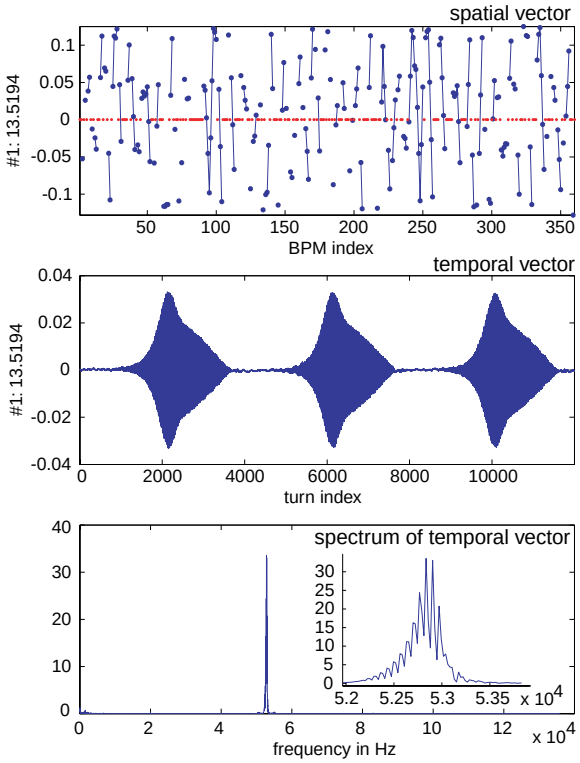

FIG. 6: Horizontal betatron mode due to instability. See caption of Fig. 1 for more description. Insert is a blowup.

three periods of the self-excited oscillation. The Fourier spectrum shows sharp clean betatron oscillation with two barely noticeable synchrotron sidebands. Detailed examination shows the betatron peak is heavily modulated at the bursting frequency. Again, using the spatial vector of this betatron mode, we calculated the phase advances and beta function. The results agree well with the results from kick excitation shown in Fig. 3. In fact, the signal is stronger than that from the kick excitation. Comparing the results from two different bursts yields repeatability of 0.7% for beta function, 0.24° for phase advances between BPMs, and 0.18° for cumulative phase. These are a little better than those with kick excitation.

E. Effects due to gradient error, energy offset, and wakefield

We have demonstrated a robust and accurate MIA technique to measure phase advances in a ring. It is well-known that phase advance (and betatron tune of course) are sensitive to various physical effects and thus its accurate measurement provides valuable information on those effects. Here we show a few such examples to demonstrate that MIA phase advance measurements can indeed be used to measure the local effects due to quadrupole gradient error, beam energy offset, and even wakefield. However, no detailed analysis will be given since it is not the focus of this paper.

Figure 7 shows the difference of two sets of horizontal phases measured under the same condition except that a quadrupole is changed by 0.5%. We see a clear 2° phase jump at the quadrupole location. Phase beating before and after the jump is also evident. The phase accuracy of this measurement is about 0.3° in rms.

Figure 8 shows horizontal phase difference due to a 100-Hz rf frequency shift (about 0.1% relative energy offset). A more or less linear increase of the phase difference shows chromatic effects. The total deviation gives a good measurement of chromatic tune shift. The local chromatic phase shift could provide information on the source of the chromatic effect. Figure 9 shows the vertical phase differences for measurements done with two different single-bunch currents at 1.1 mA and 4.9 mA. The total deviation measures the current detuning parameter often used for instability studies. Interesting local structures clearly exist. This is because the vertical gaps of the vacuum chambers vary significantly for different insertion devices. From the local phase-advance change with current, one can estimate the local reactive impedance along the ring as done at LEP [22]. We also checked the horizontal current-dependent phase difference, which shows much weaker wakefield effect and little structure other than a more or less linear decrease. This is because the horizontal aperture is much larger than the vertical one, and there is also not much variation along the ring.

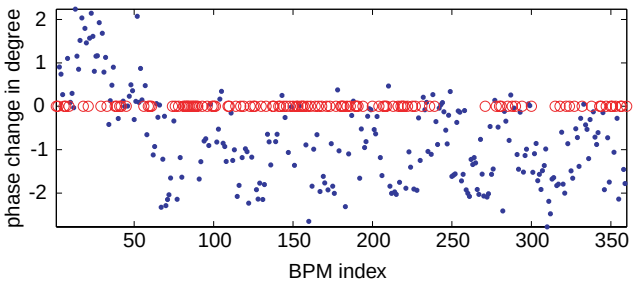

FIG. 7: Phase changes due to a 0.5% quadrupole change near the 56-th BPM. The 2° phase jump and beating pattern are evident. Again the circles indicate unusable BPMs.

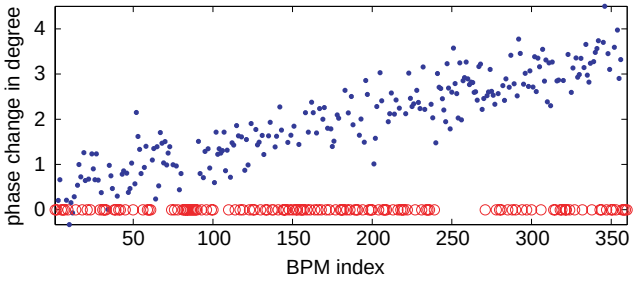

FIG. 8: Phase changes due to a 0.1% energy decrease.

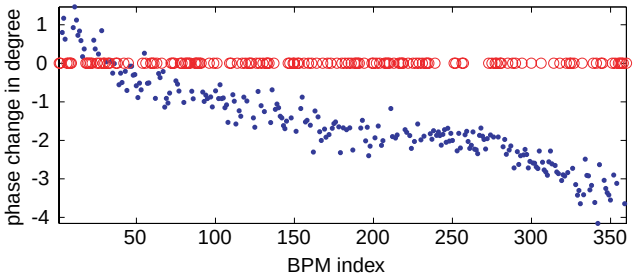

FIG. 9: Phase changes due to current-dependent wakefield.

To study the local effects in detail, it is desirable to further improve the accuracy of phase measurement. Our measurements are limited by the achievable signal strength. In the horizontal plane, the kick excitation is limited by decoherence that damps the signal within a hundred turns. In the vertical plane, the resonant excitation amplitude is currently limited to about 300 μm at low-beta BPMs and 1.2 mm at high-beta locations. In addition to improving signal strength, significant improvement may also be achieved by averaging over repeated measurements, provided that the data acquisition is fast and the machine is sufficiently stable. A preliminary test using four sets of data shows that further averaging does work. However, since our beam history system is rather slow, we did not explore further.

F. Remarks

As discussed before, the phase advance measurement is independent of machine model and BPM calibrations.

The good agreement in phase advance supports both MIA and response-matrix measurements. On the other hand, BPM gains from response-matrix fitting are used for the beta function calculation, and a fitting to the model beta function is used to determine the overall scaling factor. Furthermore, our orbit response measurements and beam history measurements use different electronic systems, thus the BPM gain calibration for one system could be different for the other. Despite these limitations in beta function measurement, the result on beta function further confirms MIA analysis.

It is desirable to be able to determine BPM gains from beam histories. Model calibration using beam histories is a promising method for determining BPM gains and transverse coupling using the same beam history measurements. However, we have not experimentally pursued this method because the large number of malfunctioning beam histories at APS makes it rather difficult if not impossible. Due to the BPM electronic systems, APS has about twice as many BPMs good for response-matrix measurements as BPMs usable for beam history measurements.

Dispersion is usually easy to measure from closed orbit change with respect to rf frequency shift. Thus we have not pursued dispersion measurement using MIA. Nonetheless, a synchrotron mode such as shown in Fig. 2 can be used to measure dispersion function. For accurate measurement, one may want to resonantly excite significant synchrotron oscillations by modulating rf phase at the synchrotron frequency, for example.

The results shown in Figs. 3 and 5 have used thousands of turns of beam history. In the horizontal case, it is actually unnecessary to use this many turns, although it helps in observing low frequency modes. The betatron signal in Fig. 1 decoheres significantly in less than a hundred turns. Thus using only a couple hundred turns gives equally good results.

We have used a few hundred BPMs in our measurements. However, our method works even if only a fraction of those BPMs are used. The measurement accuracy determined by repeatability tests showed no obvious M dependence for the vertical measurement. Nonetheless, for understanding a lattice, it is important to have a sufficiently large number BPMs to determine the beta function and phase advances.

V. CONCLUSION

We have developed and experimentally demonstrated (even with a problematic broadband BPM system) a new MIA technique to measure the phase advances of a storage ring with little coupling. Given well-calibrated BPMs, beta function can be measured as well. Compared to methods based on closed orbit measurements, our method uses beam oscillation histories that require little machine time to collect and can yield results in minutes, provided that a suitable broadband BPM system is available. Compared to the harmonic analysis of orbit oscillations, which works well only for resonantly excited clean harmonic oscillations and demands accurate tune as input, our method is much more robust and applies to all types of beam excitations. Compared to model calibration methods, our method works even when successful model calibration is prevented by an insufficient number of BPMs or lack of a good machine model. However, even though the phase advance measurement is immune from BPM gain errors, the beta function measurement does require good BPM calibration, which is a major limitation. The accuracy of our method rivals all other techniques. Since phase advances are sensitive to various physical phenomena (we demonstrated a few of them), our fast, robust, accurate, and model-independent measurement technique should be valuable to commissioning, operating, and understanding a ring. In principle this method can be adapted to linacs (by taking into account the acceleration, etc.), especially long linacs with a large number of BPMs, such as the proposed next-generation linear colliders.

Acknowledgments

We would like to acknowledge help received from colleagues and the APS operation crew during this study, especially during data acquisitions. Special thanks are due to L. Emery and M. Borland for updating the data acquisition software, G. Decker for his advice on the BPM system, and K. Harkay for helpful input on instability conditions. The first author is grateful for support from K.-J. Kim and S. Milton. This work was supported by the U.S. Department of Energy, Office of Basic Energy Sciences, under Contract No. W-31-109-ENG-38.

APPENDIX A

For convenience we use the phase-space vector $X = (x, y, x', y')^T$ instead of (x, x', y, y'). Then the Lagrange invariant $\mathcal{L}_{ij} = X_i^T J X_j$ with $J = \begin{pmatrix} 0 & I \\ -I & 0 \end{pmatrix}$, where I is a 2×2 identity matrix. Using space coordinates $z = (x, y)^T$, we have $\mathcal{L}_{ij} = z_i^T z_j' - z_j z_i'^T$. To eliminate z', we use the transfer matrix from location a to b and $z^b = R_Z z^a + R_G z'^a$, where R_Z and R_G are the 2×2 submatrices of the transfer matrix R^{ba}. Written in conventional R-matrix elements,

$$R_Z = \begin{pmatrix} R_{11}^{ba} & R_{13}^{ba} \\ R_{31}^{ba} & R_{33}^{ba} \end{pmatrix} \quad \text{and} \quad R_G = \begin{pmatrix} R_{12}^{ba} & R_{14}^{ba} \\ R_{32}^{ba} & R_{34}^{ba} \end{pmatrix}.$$

By eliminating z'^a, using $z'^a = R_G^{-1} z^b - R_G^{-1} R_Z z^a$, the Lagrange invariant can be computed with measurable quantities z^a and z^b, i.e., beam positions at two locations. The last term contributes $-(z_i^a)^T [R_G^{-1} R_Z -$

$(R_G^{-1}R_Z)^T]z_j^a$ to the invariant, where the middle anti-symmetric 2×2 matrix is easy to evaluate and yields $(R_{11}R_{32}-R_{12}R_{31}+R_{13}R_{34}-R_{14}R_{33})\begin{pmatrix}0&1\\-1&0\end{pmatrix}$, which equals zero due to the symplecticity of the R matrix. Therefore, only $R_G^{-1}R_Z$ in z'^a contributes to the Lagrange invariant and

$$\begin{aligned}\mathcal{L}_{ij} &= \left[\begin{pmatrix}I&0\\0&R_G^{-1}\end{pmatrix}\begin{pmatrix}z_i^a\\z_i^b\end{pmatrix}\right]^T J\left[\begin{pmatrix}I&0\\0&R_G^{-1}\end{pmatrix}\begin{pmatrix}z_j^a\\z_j^b\end{pmatrix}\right]\\ &= \begin{pmatrix}z_i^a\\z_i^b\end{pmatrix}^T\begin{pmatrix}0&R_G^{-1}\\-(R_G^{-1})^T&0\end{pmatrix}\begin{pmatrix}z_j^a\\z_j^b\end{pmatrix}.\end{aligned}$$

Let $Z=(z_1,z_2,z_3,z_4)$, which contains all positions of the four independent orbits and $L=(\mathcal{L}_{ij})$. Then we have a matrix equation

$$L=\begin{pmatrix}Z^a\\Z^b\end{pmatrix}^T\begin{pmatrix}0&R_G^{-1}\\-(R_G^{-1})^T&0\end{pmatrix}\begin{pmatrix}Z^a\\Z^b\end{pmatrix},$$

whose inverse yields

$$\begin{pmatrix}0&-R_G^T\\R_G&0\end{pmatrix}=\begin{pmatrix}Z^a\\Z^b\end{pmatrix}L^{-1}\begin{pmatrix}Z^a\\Z^b\end{pmatrix}^T.$$

Thus

$$R_G=\begin{pmatrix}R_{12}^{ba}&R_{14}^{ba}\\R_{32}^{ba}&R_{34}^{ba}\end{pmatrix}=Z^bL^{-1}Z^{aT}.$$

APPENDIX B

From Eq. (25) we know that the two betatron modes have approximately the same magnitudes with singular values $\sigma_\pm\simeq\sigma_s\equiv\sqrt{\langle J\rangle\langle\beta\rangle/2}$. Assume as well that the errors in $\xi_\pm=\sigma_\pm v_\pm$ are random and uncorrelated with about the same rms σ_ξ. Then from Eqs. (29, 30) we have

$$\begin{aligned}\sigma_\psi &= \sqrt{\left[\left(\frac{\partial\psi}{\partial\xi_+}\right)\sigma_{\xi_+}\right]^2+\left[\left(\frac{\partial\psi}{\partial\xi_-}\right)\sigma_{\xi_-}\right]^2}\\ &\simeq \sqrt{\left(\frac{\partial\psi}{\partial\xi_+}\right)^2+\left(\frac{\partial\psi}{\partial\xi_-}\right)^2}\,\sigma_\xi\\ &= \frac{1}{\sqrt{\xi_+^2+\xi_-^2}}\,\sigma_\xi=\sqrt{\frac{\langle J\rangle}{\beta}}\,\sigma_\xi=\sqrt{\frac{\langle\beta\rangle}{2\beta}}\,\frac{\sigma_\xi}{\sigma_s}\\ &= \sqrt{\frac{\langle\beta\rangle}{2\beta}}\,\frac{1}{\sqrt{P}}\,\frac{\sigma_r}{\sigma_s}.\end{aligned}$$

Here σ_r is the residual signal and noise magnitude, which is difficult to estimate and roughly given by the singular values beyond the betatron modes. Similarly,

$$\sigma_\beta\simeq\sqrt{\left(\frac{\partial\beta}{\partial\xi_+}\right)^2+\left(\frac{\partial\beta}{\partial\xi_-}\right)^2}\,\sigma_\xi=2\beta\,\sigma_\psi.$$

[1] J. Irwin, C.X. Wang, Y. Yan et al., *Phys. Rev. Lett.* **82**(8), 1684 (1999).

[2] Chun-xi Wang, *Model Independent Analysis of beam centroid dynamics in accelerators*, Ph.D. dissertation, Stanford University.

[3] R. Gnanadesikan, *Methods for Statistical Data Analysis of Multivariate Observations*, 2nd edition, John Wiley & Sons, inc., 1997.

[4] T. W. Anderson, *An Introduction to Multivariate Statistical Analysis*, 2nd edition, John Wiley & Sons, Inc. 1984.

[5] A. W. Chao and M. Tigner, *Handbook of Accelerator Physics and Engineering*, World Scientific Publishing Co. Ote. Ltd., 1998.

[6] F. Zimmermann, SLAC-PUB-7844, 1998.

[7] J. Borer, C. Bovet, A. Burns and G. Morpurgo, Proc. of the 3rd European Part. Accel. Conf., Berlin, March 1992, p. 1082 (1992).

[8] P. Castro and J. Borr et al., Proceedings of the 1993 Particle Accelerator Conference, p. 2103 (1993).

[9] D. Sagan, R. Meller, R. Littauer, and D. Rubin, PRST-AB **3** 092801 (2000).

[10] D. Sagan, PRST-AB **3** 102801 (2000).

[11] W.J. Corbett, M.J. Lee, and V. Ziemann, Proceedings of the 1993 Particle Accelerator Conference, p. 108 (1993).

[12] W.J. Corbett, M.J. Lee, and V. Ziemann, SPIE's 1993 International Symposium on Optics, Imaging and Instrumentation, San Diego, CA, 11-16 Jul 1993.

[13] J. Safranek, Nucl. Instr. and Meth. A**388**, 27 (1997).

[14] D. Robin, J. Safranek, G. Portmann, and H. Nishimura, Proceedings of the 1996 European Particle Accelerator Conference, p.971 (1996).

[15] V. Sajaev and L. Emery, Proceedings of the 2002 European Particle Accelerator Conference, p. 742 (2002).

[16] J. Irwin and Y.T. Yan, Proceedings of the 2000 European Particle Accelerator Conference, p. 151 (2000).

[17] Y. Cai, J. Irwin, M. Sullivan, and Y.T. Yan, Proceedings of the 2001 Particle Accelerator Conference, p. 3555 (2001).

[18] See, for example, H. Wiedemann, *Particle Accelerator Physics II*, 2nd ed., Springer-Verlag, 1999.

[19] Gene H. Golub and Charles F. Van Loan, *Matrix Computations*, 3rd edition, p. 451, The Johns Hopkins University Press 1996.

[20] Chun-xi Wang, Michael Borland, Vadim Sajaev, and Kwang-Je Kim, Proceedings of the 2001 Particle Accelerator Conference, p. 1355 (2001).

[21] K. Harkay, Z. Huang, E. Lessner, and B. Yang, Proceedings of the 2001 Particle Accelerator Conference, p. 1915 (2001).

[22] D. Brandt et al., Proceedings of the 1995 Particle Accelerator Conference, p. 570 (1995).